

UNAVAILABLE  
~~CONFIDENTIAL~~C.1  
Copy 5  
RM E52E15

NACA RM E52E15

NACA

## RESEARCH MEMORANDUM

INVESTIGATION OF LOSSES IN THE XJ35-A-23

TWO-STAGE TURBINE

By John J. Rebeske, Jr., and Robert E. Forrette

Lewis Flight Propulsion Laboratory  
Cleveland, Ohio

FOR REFERENCE

CLASSIFICATION CHANGED

NOT TO BE TAKEN FROM THIS BOOK

UNAVAILABLE

To UNCLASSIFIED

By authority of *7 ACA Rec. abv*  
*+ RM-115*Date *effective*  
*7-8-57*

at 5-23-57

CLASSIFIED DOCUMENT

This material contains information affecting the National Defense of the United States within the meaning of the espionage laws, Title 18, U.S.C., Secs. 793 and 794, the transmission or revelation of which in any manner to an unauthorized person is prohibited by law.

NATIONAL ADVISORY COMMITTEE  
FOR AERONAUTICS

WASHINGTON

August 18, 1952

~~CONFIDENTIAL~~

UNAVAILABLE

NACA LIBRARY

U.S. GOVERNMENT PRINTING OFFICE: 1952 O - 484,000



## NATIONAL ADVISORY COMMITTEE FOR AERONAUTICS

RESEARCH MEMORANDUM

## INVESTIGATION OF LOSSES IN THE XJ35-A-23 TWO-STAGE TURBINE

By John J. Rebeske, Jr., and Robert E. Forrette

SUMMARY

Inasmuch as design performance was not obtained from the XJ35-A-23 two-stage turbine, an investigation of the stage work distribution and the losses through the turbine at design conditions was made.

This investigation showed that the poor performance of this turbine was primarily due to: large whirl velocities at the turbine exit, which caused a 4-percent loss in turbine efficiency; choking in the second-stage rotor, which limited the work output of the first stage and the velocities out of the second-stage stator; and a choking condition upstream of the physical blade throat, which caused excessive losses in the second-stage rotor blades. Consequently, a satisfactory two-stage turbine can be obtained if these unfavorable conditions are eliminated.

INTRODUCTION

As part of a general study of high-work-output low-speed multistage turbines, a two-stage turbine for the XJ35-A-23 turbojet engine was studied at the NACA Lewis laboratory. The over-all performance of this turbine is reported in reference 1. Limiting blade loading (reference 2) occurred in the second-stage rotor of this turbine and limited the maximum turbine work output to 95 percent of the design value; the efficiency of the turbine at this point was only 0.75.

In order to determine why design performance was not obtained from this turbine, interstage instrumentation was added to the experimental apparatus. The turbine was operated at equivalent design speed and pressure ratio and detailed flow measurements were recorded. From an examination of the turbine design and these detailed flow measurements, the major losses in the turbine were located. The probable causes of these losses are presented and discussed. The present report is concerned only with a general qualitative evaluation of the principal losses associated with the turbine and, in general, these losses appear as a loss in stagnation pressure at various points through the turbine.

## SYMBOLS

The following symbols are used in this report:

A	annular area, sq ft
a	local speed of sound, $\sqrt{\gamma gRT}$ , ft/sec
$c_p$	specific heat at constant pressure, Btu/(lb)(°R)
$c_v$	specific heat at constant volume, Btu/(lb)(°R)
E	shaft work based on torque measurements, Btu/lb
g	acceleration due to gravity, 32.174 ft/sec <sup>2</sup>
$\Delta H$	enthalpy change based on stagnation temperature, $c_p \Delta T'$ , Btu/lb
J	mechanical equivalent of heat, 778.2 ft-lb/Btu
N	rotational speed, rpm
$\frac{N}{\sqrt{\theta_{cr}}}$	equivalent rotational speed, rpm
p	static pressure, lb/sq ft
p'	stagnation pressure, lb/sq ft
$p'_x$	stagnation pressure based on axial component of velocity, lb/sq ft
R	gas constant, ft-lb/(lb)(°R)
r	radius, ft
T	static temperature, °R
T'	stagnation temperature, °R
T''	relative stagnation temperature, °R
u	blade velocity, ft/sec
V	absolute gas velocity, ft/sec
$V_{cr}$	critical gas velocity, $\sqrt{\frac{2\gamma}{\gamma+1} gRT'}$ , ft/sec

$W$  gas velocity relative to rotor, ft/sec

$W_{cr}$  relative critical gas velocity,  $\sqrt{\frac{2r}{r+1} gRT''}$ , ft/sec

$w$  weight flow, lb/sec

$\frac{w \sqrt{\theta_{cr}}}{\delta} \beta$  equivalent weight flow, lb/sec

$\beta$  function of  $r$ , 
$$\frac{r_0}{r_e} \left[ \frac{\left( \frac{r_e+1}{r_e} \right)^{\frac{r_e}{r_e-1}}}{\left( \frac{r_0+1}{r_0} \right)^{\frac{r_0}{r_0-1}}} \right]$$

$\gamma$  ratio of specific heats,  $c_p/c_v$

$\delta$  ratio of inlet pressure to pressure at NACA standard sea-level conditions,  $p'/p'_{x,5}$

$\eta_{ad}$  adiabatic efficiency based on stagnation-temperature ratio and stagnation-pressure ratio

$\eta_i$  brake internal efficiency defined as ratio of actual turbine work based on torque measurements to ideal turbine work based on the pressure ratio  $p'_1/p'_{x,5}$

$\theta_{cr}$   $\left( \frac{V_{cr}}{V_{cr,0}} \right)^2$

$\theta''_{cr}$   $\left( \frac{W_{cr}}{W_{cr,0}} \right)^2$

$\rho$  gas density, lb/ft<sup>3</sup>

$\bar{\omega}$  stagnation-pressure-loss coefficient,  $\Delta p'/(p'-p)$

## Subscripts:

1,2,3,4,5	instrument locations (see fig. 1)
( ) <sub>av</sub>	weight-flow-average value of parameter
e	engine operating conditions
h	hub
s	isentropic
t	tip
u	tangential
x	axial
0	NACA standard sea-level conditions

2531

## INSTRUMENTATION

The experimental apparatus and the installation are described in reference 1. The air weight flow through the turbine was measured by a submerged A.S.M.E. flange-tap flat-plate orifice. Two standard jet-engine burners were used to heat the air to 700° R, and the fuel flow to the burners was measured by rotameters in the fuel line.

The location of measuring stations through the turbine and the type of measurements made at each station are shown in figure 1. The turbine inlet conditions were measured by means of a combination probe consisting of a shielded stagnation-pressure tube and a calibrated thermocouple, and two static-pressure taps in each of the ten standard transition sections. The turbine exit conditions were determined by means of four calibrated thermocouple rakes, each consisting of five thermocouples located at the area centers of five equal annular areas; five shielded stagnation-pressure probes, located at different circumferential positions and radii corresponding to the area centers of the five equal annular areas; and four static-pressure taps on both the inner and the outer shrouds.

The instrumentation used to obtain the survey data was as follows:

(1) Movable unshielded stagnation-pressure probes with provision for angle measurement (a claw-type probe), to measure stagnation pressures and flow angles

(2) Wall static taps, to measure static pressures

(3) Fixed thermocouple rakes, each consisting of five thermocouples located at the area centers of five equal annular areas, to measure stagnation temperatures

#### METHODS AND PROCEDURE FOR EXPERIMENTAL EVALUATION OF TURBINE LOSSES

Detailed survey data were obtained by operating the turbine at equivalent design speed (3028 rpm) and equivalent design pressure ratio (4.03). The inlet conditions were maintained at an inlet temperature of 700° R and an inlet stagnation pressure of 40 inches of mercury absolute.

Turbine efficiencies. - The brake internal turbine efficiency was calculated from measurements of torque and turbine exit conditions of stagnation pressure and temperature, static pressure, and weight flow. It is defined as

$$\eta_i = \frac{E}{c_p T_1 \left[ 1 - \left( \frac{p'_{x,5}}{p_1} \right)^{\frac{\gamma-1}{\gamma}} \right]} \quad (1)$$

where  $p'_{x,5}/p_1$  is a pressure ratio based on the axial component of velocity at the turbine exit. This ratio can be derived from a combination of the following equations:

Continuity:

$$w = \rho_5 A_5 V_{x,5} \quad (2)$$

State:

$$p_5 = \rho_5 R T_5 \quad (3)$$

Energy:

$$\frac{T_1}{T_5} = 1 + \left( \frac{\gamma-1}{2} \right) \left( \frac{V_5}{a_5} \right)^2 \quad (4)$$

Isentropic relation:

$$\frac{p'_5}{p_5} = \left( \frac{T'_5}{T_5} \right)^{\frac{\gamma}{\gamma-1}} \quad (5)$$

Combining equations (2), (3), and (5) gives an equation for the axial velocity

$$V_{x,5} = \left( \frac{w}{A_5} \right) \frac{RT_5^{\frac{1}{\gamma}}}{P_5^{\frac{1}{\gamma}}} \left( \frac{P_5'}{P_5} \right)^{\frac{1}{\gamma}} \quad (6)$$

This velocity is used in the energy equation to calculate  $P_{x,5}'$ , neglecting the tangential component of velocity at the turbine exit. From equations (4) and (5),

$$P_{x,5}' = P_5 \left[ 1 + \frac{\gamma-1}{2\gamma R} \frac{V_{x,5}^2}{T_5^{\frac{\gamma-1}{\gamma}}} \left( \frac{P_5'}{P_5} \right)^{\frac{\gamma-1}{\gamma}} \right]^{\frac{\gamma}{\gamma-1}} \quad (7)$$

From this relation,  $P_{x,5}'/P_1$  is obtained and used in equation (1) to calculate  $\eta_1$ . Thus, the kinetic energy contained in the exit tangential velocity component is considered a loss.

The adiabatic efficiency for radial positions corresponding to constant percentage values of annular area of each stage of the turbine was calculated from survey measurements of stagnation pressure and temperature by the equation

$$\eta_{ad,1-3} = \frac{1 - \frac{T_3'}{T_1'}}{1 - \left( \frac{P_3'}{P_1'} \right)^{\frac{\gamma}{\gamma-1}}} \quad (8)$$

(These subscripts refer to the first stage.)

Pressure-loss coefficient. - The pressure-loss coefficient is defined as the ratio of the stagnation-pressure drop across a blade row to the difference between the stagnation pressure and the static pressure at the exit of the blade row

$$\bar{\omega}_{1-2} = \frac{P_1' - P_2'}{P_2' - P_2} \quad (9)$$

This coefficient is used in the present report only to evaluate the stagnation-pressure losses in the first- and the second-stage stators.

Weight-flow-average values. - In order to aid in the discussion and comparison of the various parameters used in the data analyses, weight-flow-average values were calculated. For example, if the weight-flow-average value of the pressure-loss coefficient  $(\bar{w})_{av}$  is required, it can be expressed as

$$(\bar{w})_{av} = \frac{\int_0^A \bar{w} \rho V_x dA}{\int_0^A \rho V_x dA} \quad (10)$$

The value of  $(\bar{w})_{av}$  is obtained by plotting the numerator and the denominator of equation (10) as a function of percentage annular area and integrating numerically. The same method is used in calculating weight-flow-average values of the other parameters.

## RESULTS AND DISCUSSION

From the over-all performance of the two-stage turbine presented in reference 1, the following turbine performance characteristics are noted:

- (1) Measured equivalent weight flow was 106 percent of the design value.
- (2) Limiting blade loading occurred in the second-stage rotor at equivalent design speed and pressure ratio and restricted the equivalent work output to approximately 95 percent of the design value.
- (3) Turbine efficiency  $\eta_1$  at equivalent design speed and pressure ratio was only 0.75.

The reason design performance was not obtained from this turbine can be determined from a study of the stage work distribution and losses through the turbine. The work distribution and the losses are evaluated on the basis of the turbine design and on the actual turbine performance.

Loss due to exit whirl. - An examination of the turbine design velocity diagrams (fig. 2) reveals only one source of turbine loss. This is the loss of kinetic energy associated with the whirl velocity at the exit of the second rotor. The kinetic energy of this whirl velocity



taken at the pitch line at the exit of the second rotor is approximately 4 percent of the isentropic enthalpy drop through the turbine. Because no provision is made for recovery of this energy, it represents approximately a 4-percent loss in turbine efficiency.

The actual loss due to exit whirl was determined experimentally and the results are shown in figure 3. The ratio of the kinetic energy contained in the tangential component of exit velocity  $V_{u,5}$  to the isentropic enthalpy drop based on the measured stagnation-pressure ratio is presented for several radial positions across the blade span. The weight-flow-average value of this ratio is approximately 4 percent of the available isentropic enthalpy drop and consequently represents a 4-percent loss in turbine efficiency  $\eta_1$ .

Stage work distribution. - The variation of the stage work parameter  $\Delta T'/T'$  along the blade radius (expressed as a percentage of the total annular area) for both the first and the second stages is shown in figure 4. In figure 4(a), a peak value of  $\Delta T'/T'$  of 0.126 occurs at a radial position corresponding to 40 percent of the annular area. From this point, the value decreases toward the hub and the tip of the blade. The weight-flow-average value of  $\Delta T'/T'$  for this stage is 0.1153 and is represented by the dashed line on the figure. In figure 4(b), a peak value of  $\Delta T'/T'$  for the second stage of 0.1630 occurs at a radial position corresponding to 50 percent of the annular area and decreases sharply toward the hub and the tip of the blade. The weight-flow-average value of  $\Delta T'/T'$  for the second stage is 0.1368. The corresponding design value of  $\Delta T'/T'$  for each stage based on the equivalent design value of  $\Delta H/\theta_{cr}$  (32.4 Btu/lb) and the design work distribution between stages (0.53 and 0.47) is 0.138 and 0.142 for the first and the second stages, respectively. The percentage of the equivalent design stage work  $\Delta T'/T'$  actually obtained from the turbine is 83.7 percent for the first stage and 96.3 percent for the second stage.

Although the measured equivalent weight flow was 106 percent of the design value, stator-exit design velocities were not obtained. This fact indicates that the design area of the first stator was too large with the result that the first-stage work output was lower than the design value. Another condition that contributed to the deficiency of work in the first stage was that the actual area of the first-stage stator was 2 percent larger than the design value.

However, choking in the second-stage rotor at a pressure ratio less than the design pressure ratio was the principal cause for the deficiency in over-all turbine work. Figure 5 (fig. 4, reference 1) shows the variation in equivalent weight flow at the turbine inlet with over-all turbine pressure ratio for a range of equivalent rotor speeds. The value of choking equivalent weight flow varies with rotor speed, the

value decreasing as the equivalent rotor speed increases. The turbine is therefore choked downstream of the first-stage stator. Figure 6 shows the variation of equivalent weight flow, calculated for stagnation conditions relative to the second-stage rotor, with over-all turbine pressure ratio for equivalent rotor speeds corresponding to 100, 110, 120, and 130 percent of the design speed. The choking value of equivalent weight flow occurs at over-all turbine pressure ratios higher than 3.6 and exhibits no significant variation with equivalent rotor speed. The variation in the value of choking weight flow for the four equivalent speeds shown is less than 1 percent, which is within the limits of experimental error. As a result, the second-stage rotor limits the weight flow through the turbine at over-all turbine pressure ratios greater than 3.6.

Because the second-stage rotor chokes, a further increase in pressure ratio across any upstream blade row cannot be obtained. Consequently, the work output of the first stage is limited, and no velocity increase can be obtained through the second-stage stator. Further increase in turbine work output with increase in over-all turbine pressure ratio is due to an increase in the tangential component of exit velocity. This component reaches a maximum value at the condition of limiting blade loading, and further increase in over-all turbine pressure ratio produces no additional work.

Stage efficiencies. - The radial variation in the efficiency  $\eta_{ad}$  for the first stage is shown in figure 7(a). A peak stage efficiency of 94.0 percent occurs at a radial position corresponding to approximately 40 percent of the total annular area. From this point, the efficiency decreases toward the hub and the tip of the blade. The weight-flow-average value of this efficiency is 83.3 percent and is represented by the dashed line on the figure. In order to determine the losses in the first-stage stator, a pressure-loss coefficient  $\bar{w}$  is evaluated between the turbine inlet (station 1, fig. 1) and the exit of the first stator (station 2, fig. 1). The radial variation of this pressure-loss coefficient is shown in figure 7(b). The pressure-loss coefficient increases rapidly from a minimum value of 0.0245 at 15 percent of the annular area to a value of 0.143 at the tip of the blade. The weight-flow-average value of this pressure-loss coefficient  $(\bar{w})_{av,1-2}$  is 0.0765. The increasing values of the pressure-loss coefficient as the stator blade tip is approached indicate that part of the over-all turbine loss occurs in the inlet geometry of the turbine and also explains the decrease in stage efficiency towards the tip of the first rotor blade. Near the hub of the first-stage stator the pressure-loss coefficient is low; consequently, the decrease in stage efficiency near the hub is due to losses in the first-stage rotor near the hub.

The radial variation in efficiency of the second stage is shown in figure 8(a). A peak value of 82.0 percent occurs at 50 percent of the

annular area. The efficiency decreases rapidly toward the hub and the tip of the blade. The weight-flow-average value of the efficiency for this stage is 66.0 percent and is represented by the dashed line on the figure. Figure 8(b) shows the spanwise variation in the pressure-loss coefficient across the second-stage stator (evaluated between stations 3 and 4, fig. 1). A maximum value of 0.037 occurs at a spanwise position corresponding to 55 percent of the annular area and decreases to negative values near the hub and tip of the blade. The negative values indicate a stagnation-pressure rise and are probably due to secondary flows which caused a redistribution of the mass flow through this stator. The weight-flow-average value of the pressure-loss coefficient for this stator is 0.0112 and is represented by the dashed line on the figure. Because the value of the pressure-loss coefficient across the second-stage stator is low and because the second-stage efficiency is also low, large losses are indicated in the second-stage rotor.

Loss in second-stage rotor. - In an effort to determine the cause of the large losses across this rotor, a stream filament analysis (reference 3) of the flow through this blade row was made at the hub, the mean, and the tip radius of the blade. This analysis was based on the design velocity diagrams and showed that this rotor would not pass the design weight flow. This result is verified by the experimental data which show that this rotor chokes at a pressure ratio less than design pressure ratio. The analysis also indicated that the choking condition occurred upstream of the physical throat (minimum geometric area). Figure 9 shows the variation of the geometric and the effective flow area ratios with percentage of hub blade chord. The method used to determine these area ratios is presented in the appendix. At approximately 94 percent of axial chord at the hub, the effective area ratio is 1.02 as compared with 1.00 for the geometric area ratio. Because the effective and geometric areas are approximately equal at this point, the minimum effective area is approximately 2 percent smaller than the minimum geometric area. The figure also shows that the geometric area ratio decreases through the blade row, whereas the effective area ratio reaches a minimum value at 45 percent of the axial chord. This converging-diverging area variation results in high losses for outlet Mach numbers of the order of 1.0. For normal reaction and impulse blades, the profile pressure-loss coefficient generally decreases as an outlet Mach number of 1.0 is approached (fig. 63, p. 233, reference 4). If the blade has a minimum effective area upstream of the trailing edge, however, large pressure-loss coefficients will result (fig. 16, reference 5). The probable cause for this increase in the pressure-loss coefficient is that shocks on the suction surface cause a local static-pressure rise which induces flow separation from the suction surface of the blade, especially if there is appreciable curvature of the suction surface downstream of the choke point (fig. 12, reference 6).

In order to reduce the high losses in the second-stage rotor, the blade profiles should be designed so that the effective area decreases through the blade passage.

## SUMMARY OF RESULTS

Inasmuch as design performance was not obtained from the XJ35-A-23 two-stage turbine, an investigation of the stage work distribution and the losses through the turbine at design conditions was made. This investigation showed that:

1. The loss due to the whirl velocity at the turbine exit, based on actual turbine performance, was approximately 4 percent of the available isentropic enthalpy drop through the turbine.
2. Choking in the second-stage rotor limited the work output of the first stage and the velocities out of the second-stage stator at over-all turbine pressure ratios above 3.6.
3. Choking in the second-stage rotor blades upstream of the physical blade throat induced large losses in this blade row.

## CONCLUDING REMARKS

The results obtained from a study of the losses through this two-stage turbine indicate that the poor performance is primarily due to the unfavorable choking conditions in the second-stage rotor and the loss of energy contained in the exit whirl velocity. Consequently, a satisfactory two-stage turbine can be obtained if these unfavorable conditions are eliminated.

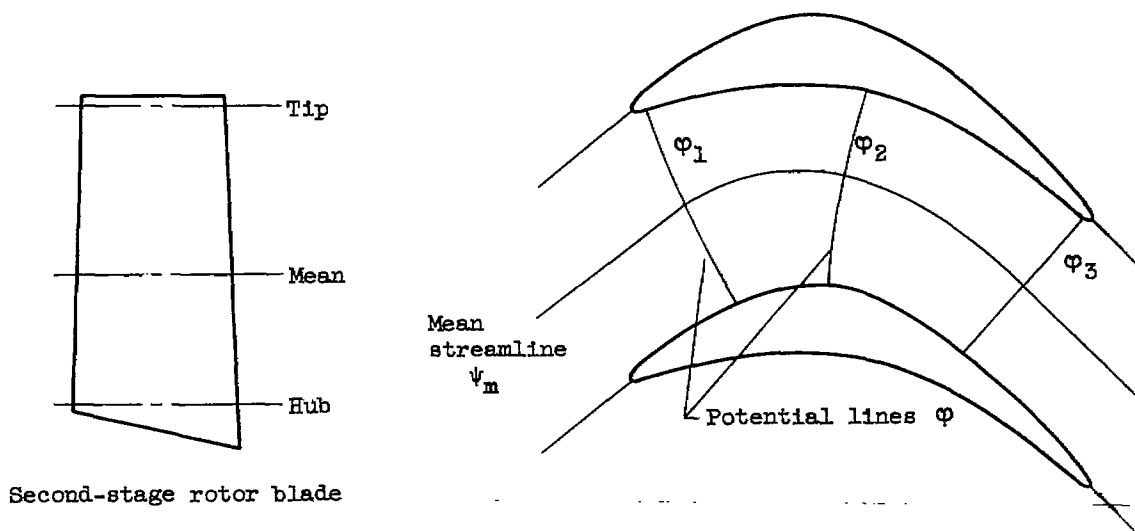
Lewis Flight Propulsion Laboratory  
National Advisory Committee for Aeronautics  
Cleveland, Ohio

## APPENDIX - DETERMINATION OF AREA VARIATIONS WITH PERCENTAGE

## OF AXIAL BLADE CHORD AT HUB

## Geometric Area Variation

The geometric area variation was determined by first making a blade passage layout to scale as indicated in the following sketch:



This layout was made for constant values of hub, mean, and tip radius at the leading edge of the blade row. The orthogonal system of streamlines  $\psi$  and velocity potential lines  $\phi$  was then sketched in. The lengths of the velocity potential lines were measured and are designated by the symbol  $n_o$ . The  $n_o$ -values through the blade passage were thus determined for the hub, the mean, and the tip radius of the blade. From the blade geometry, the intersections of the  $\phi$ -lines with the mean passage streamline  $\psi_m$  were located. The  $n_o$ -values for the hub, the mean, and the tip radius were then plotted against the corresponding percentage value of the axial chord. Values of  $n_o$  at constant percentage values of the axial chord were then read and plotted against radius. A trapezoidal integration between the hub and the tip radius was used to determine the

value of the integral  $\int_{r_h}^{r_t} n_o dr$  for each constant percentage value of

axial blade chord. The variation of the lower limit  $r_h$  of this integral with the percentage of chord due to the divergence of the inner shroud was considered in the evaluation of this integral. Each integral value thus determined was then plotted against the corresponding percentage value of axial blade chord at the hub. Each of these values was then divided by the minimum integral value obtained and this ratio is presented in figure 9.

#### Effective Area Variation

The parameter  $\mu$  is defined (reference 3, p. 16) as a function of the geometry of the blade passage and the flow velocity and can be written relative to the rotor and in gravitational units as

$$\mu = \frac{w}{\rho'' n_0 \sqrt{\frac{2\gamma}{\gamma-1} gRT''}} \quad (A1)$$

where

$w$  weight flow per unit depth flowing across velocity potential line, lb/(sec)(ft)

$n_0$  distance across velocity potential line, ft

$\rho''$  stagnation density relative to rotor, lb/ft<sup>3</sup>

By the calculation of various parameters which are functions of the geometry of the blade passage, the choking value of  $\mu$  for each velocity potential line was determined by the method of reference 3 (p. 17 and fig. 14). This choking value of  $\mu$ , when multiplied by its corresponding value of  $n_0$ , represents the choking value of the weight flow per unit depth for the particular velocity potential line. The value of  $(\mu n_0)_c$  thus determined is proportional to an effective choking area.

A plot of these choking values  $(\mu n_0)_c$  against percentage of axial blade chord at the hub was then used to calculate the values of

$\int_{r_h}^{r_t} (\mu n_0)_c dr$  by the same procedure as outlined in the preceding section.

The ratio of these integral values to the minimum integral value plotted against percentage of axial blade chord at the hub represents an effective area ratio variation through the blade passage. This variation is shown in figure 9.

## REFERENCES

1. Rebeske, John J. Jr., Berkey, William E., and Forrette, Robert E.: Over-all Performance of J35-A-23 Two-Stage Turbine. NACA RM E51E22, 1951.
2. Hauser, Cavour H., and Plohr, Henry W.: Two-Dimensional Cascade Investigation of the Maximum Exit Tangential Velocity Component and Other Flow Conditions at the Exit of Several Turbine Blade Designs at Supercritical Pressure Ratios. NACA RM E51F12, 1951.
3. Huppert, M. C., and MacGregor, Charles: Comparison Between Predicted and Observed Performance of Gas-Turbine Stator Blade Designed for Free-Vortex Flow. NACA TN 1810, 1949.
4. Ainley, D. G.: Performance of Axial-flow Turbines. Lectures on the Development of Internal Combustion Turbines. Published in War Emergency Issue no. 41 by Inst. Mech. Eng. (London). (Reprinted in U.S. by A.S.M.E., April 1949, pp. 230-244.)
5. Stanitz, John D., and Sheldrake, Leonard J.: Application of a Channel Design Method to High-Solidity Cascades and Tests of an Impulse Cascade with  $90^\circ$  of Turning. NACA TN 2652, 1952.
6. Ainley, D. G., and Mathieson, G. C. R.: An Examination of the Flow and Pressure Losses in Blade Rows of Axial Flow Turbines. Rep. no. R. 86, British N.G.T.E., March 1951.

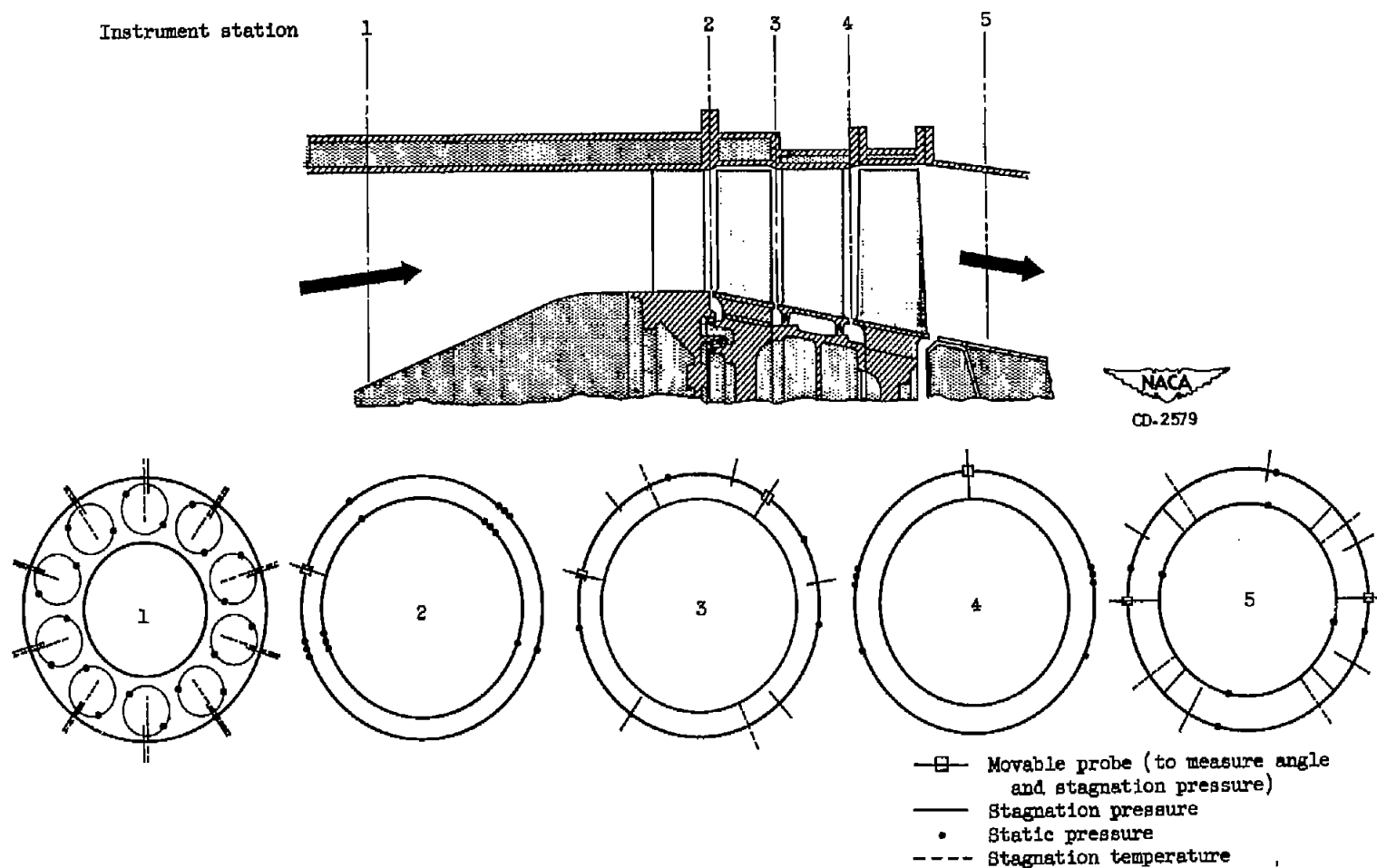


Figure 1. - Schematic diagram of XJ35-A-23 turbine in a radial-axial plane showing instrument stations and location of instruments at each instrument station.



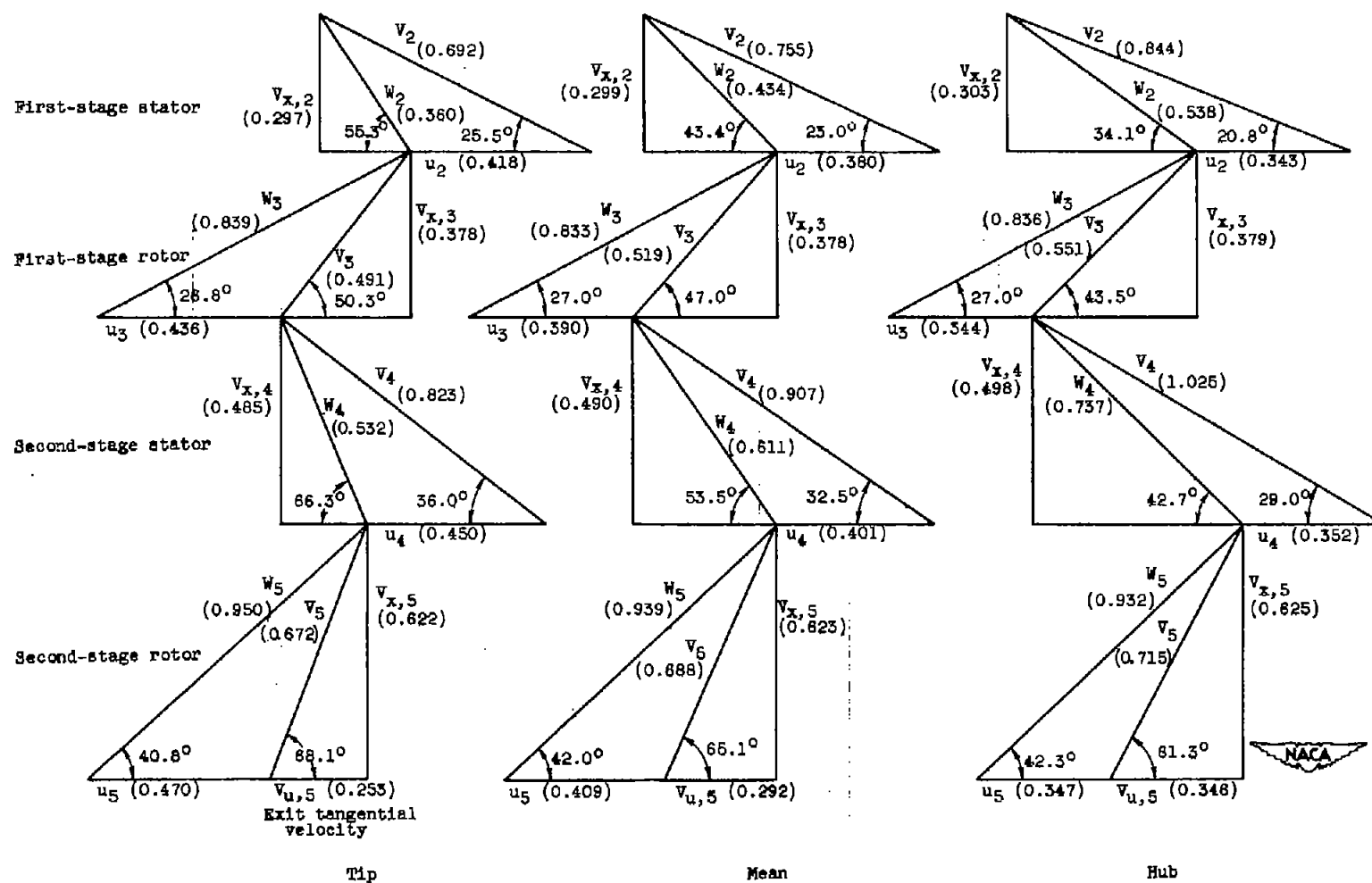


Figure 2. - Velocity vector diagrams for IJ35-A-23 two-stage turbine (design values). Engine design conditions: inlet temperature,  $2160^\circ \text{R}$ ; specific heat at constant pressure, 0.283 Btu per pound per  $^\circ \text{R}$ ; ratio of specific heats, 1.32; over-all enthalpy change, 131.2 Btu per pound; stage work split, 53 and 47 percent. Mach numbers are given in parentheses.

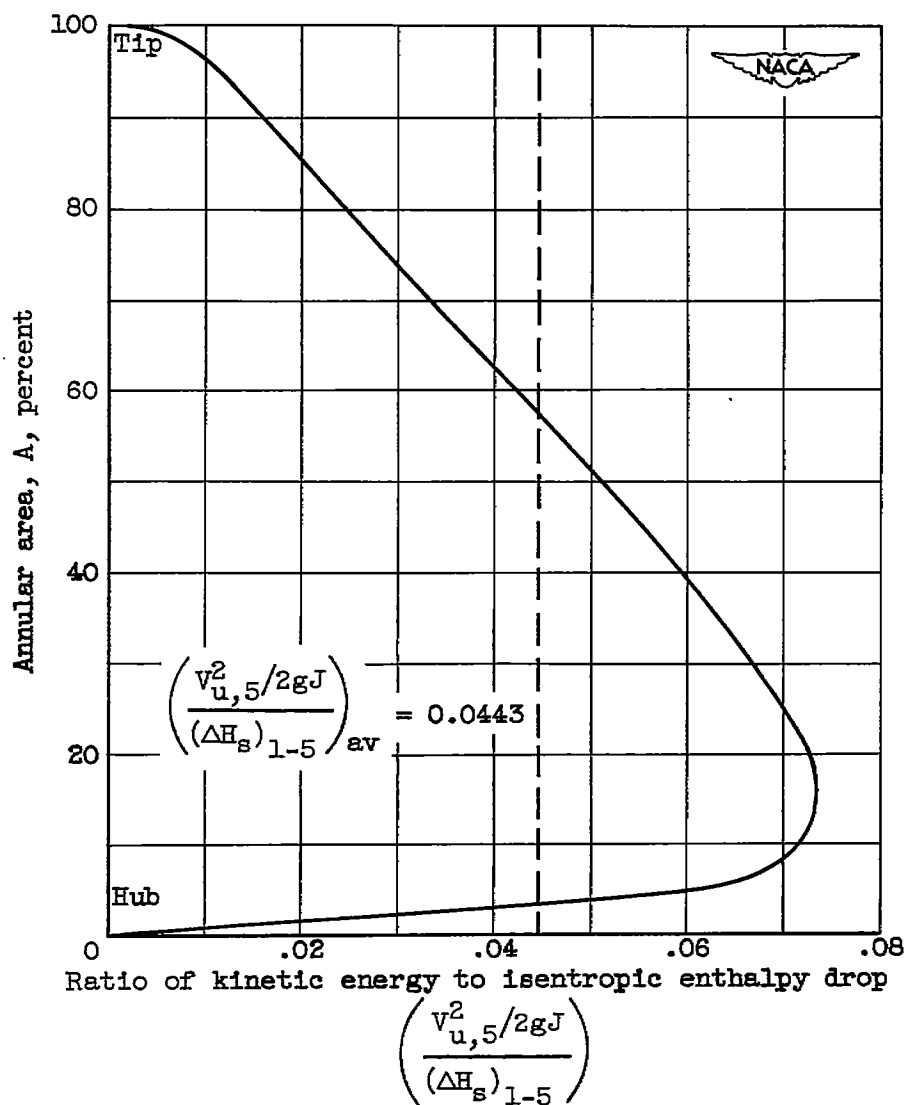


Figure 3. - Spanwise variation in ratio of kinetic energy contained in tangential component of velocity at turbine exit to available isentropic enthalpy drop through turbine for equivalent design speed and pressure ratio.

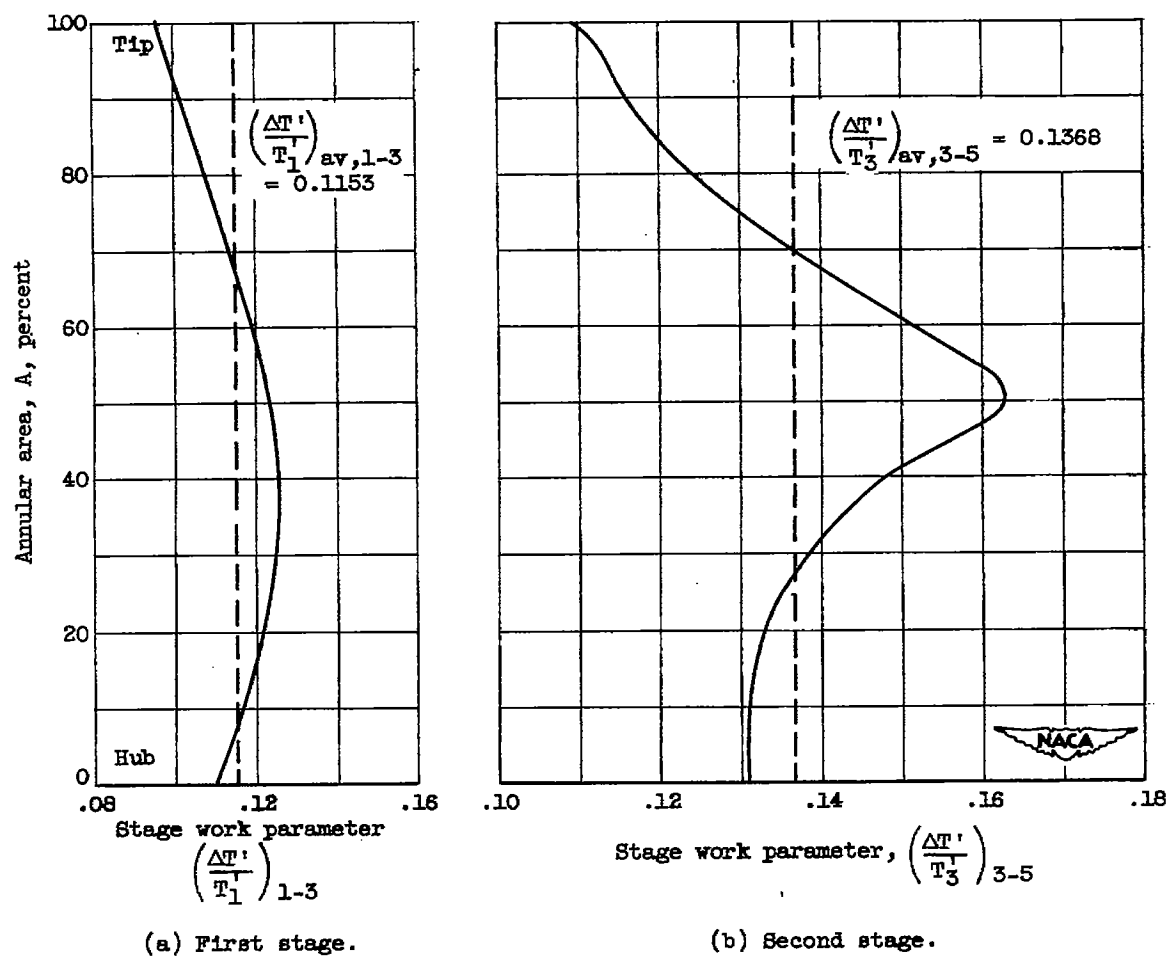


Figure 4. - Spanwise variation in stage work for equivalent design speed and pressure ratio.

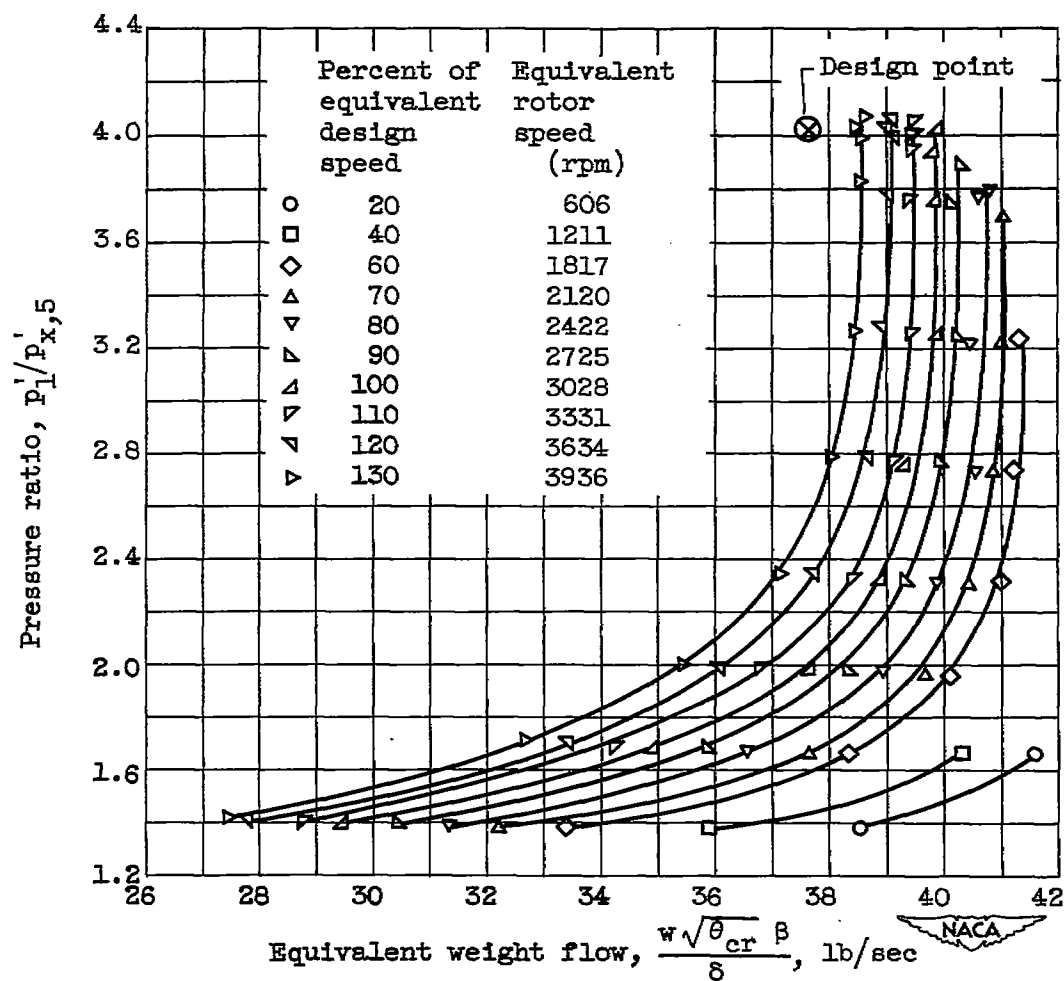


Figure 5. - Variation of equivalent weight flow with pressure ratio for various turbine speeds.

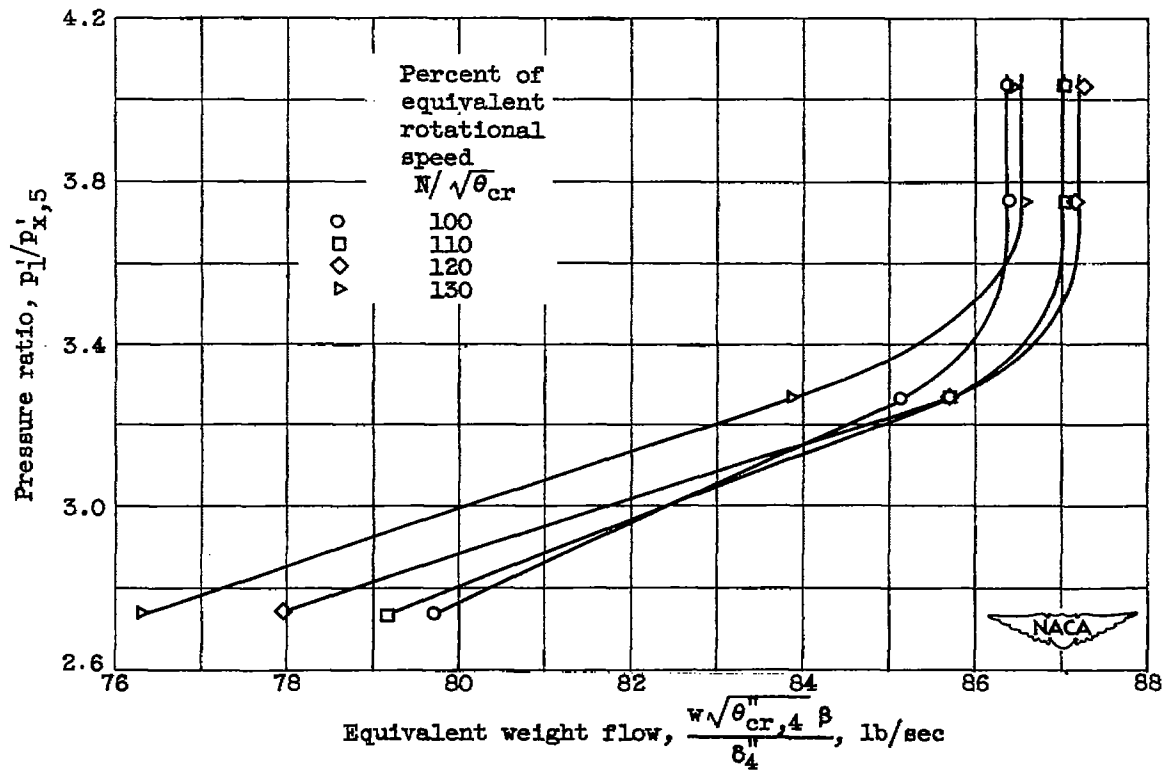
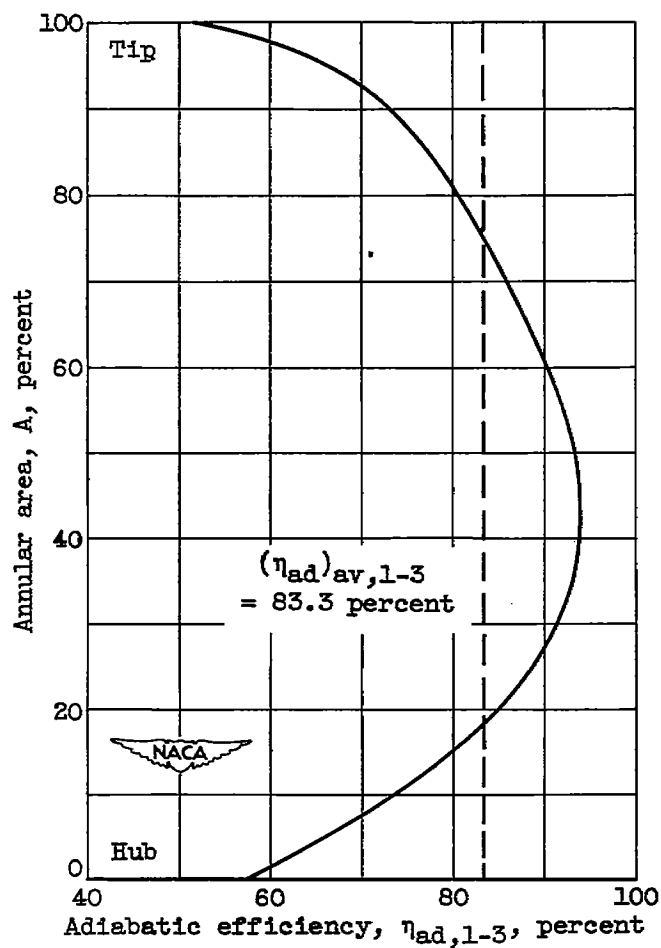
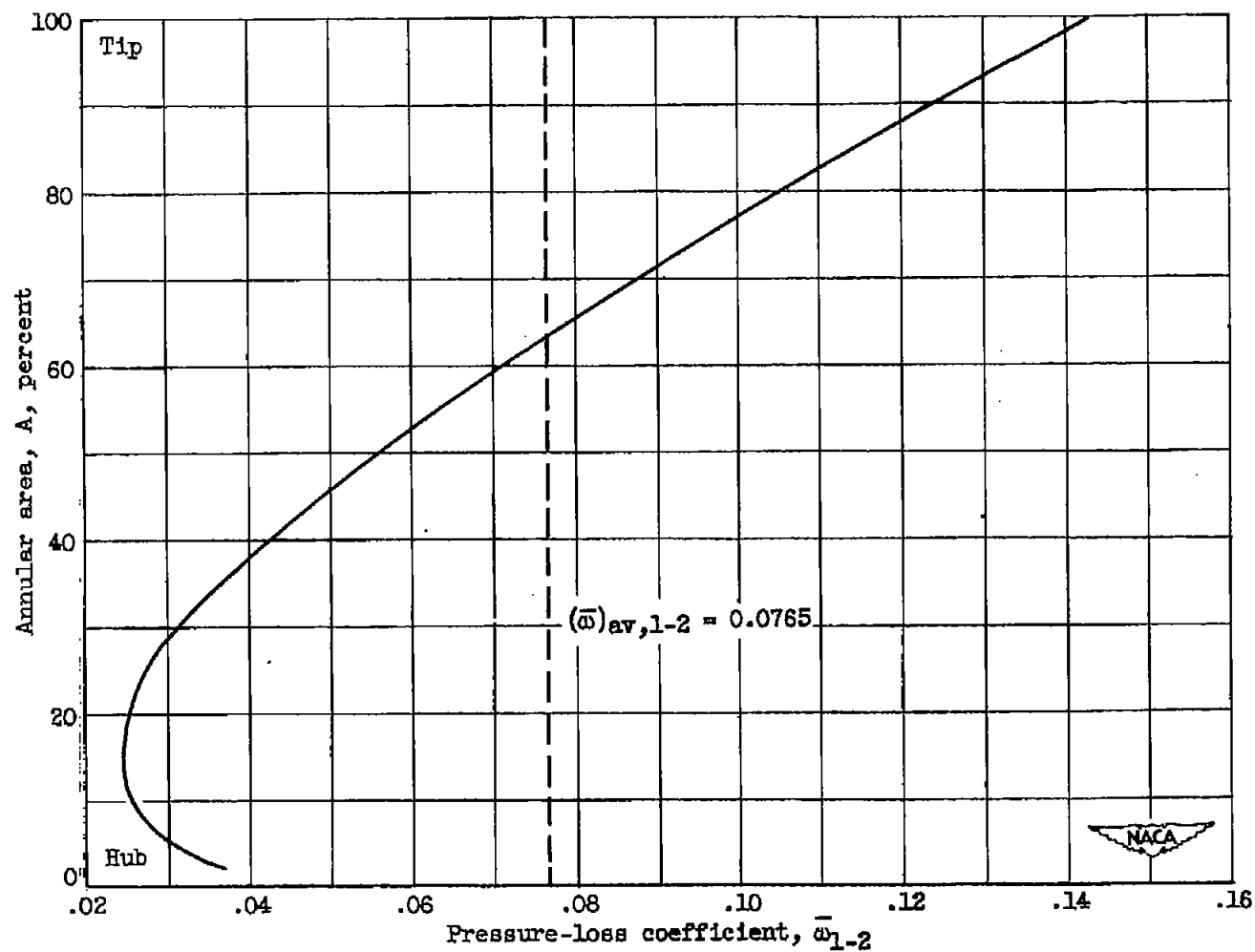


Figure 6. - Variation of equivalent weight flow relative to second-stage rotor with over-all turbine pressure ratio for range of equivalent rotor speeds.



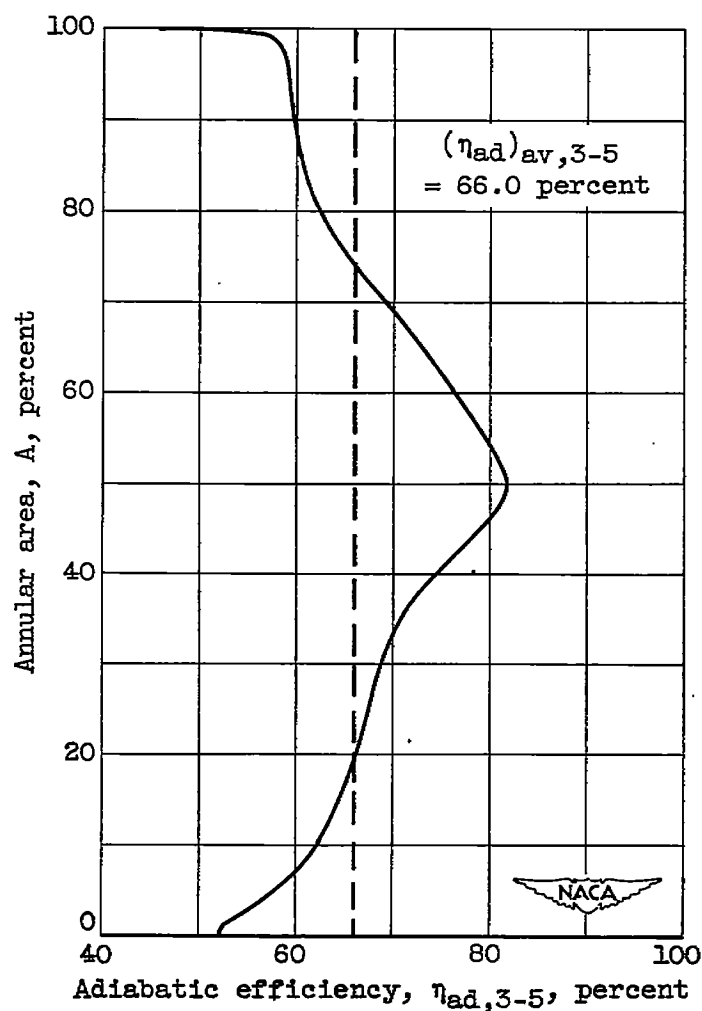
(a) Adiabatic efficiency.

Figure 7. - Spanwise variation of adiabatic efficiency and pressure-loss coefficient in first stage for equivalent design speed and pressure ratio.



(b) Pressure-loss coefficient across stator.

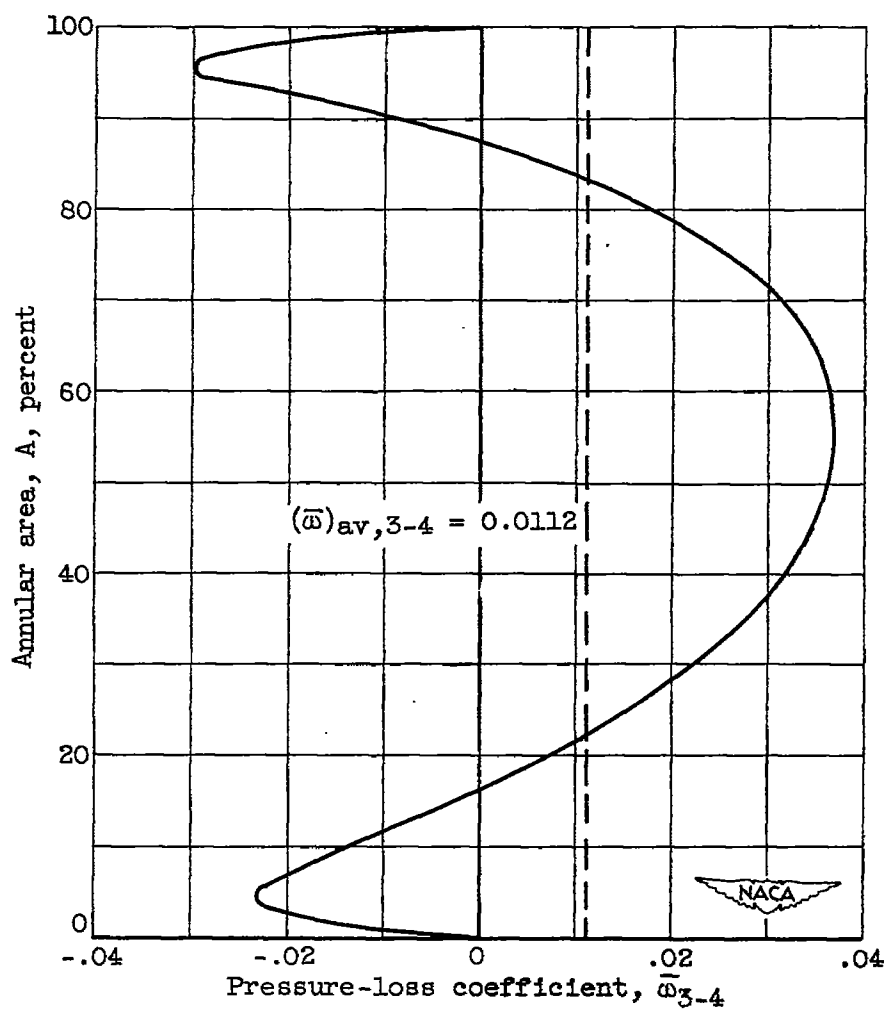
Figure 7. - Concluded. Spanwise variation of adiabatic efficiency and pressure-loss coefficient in first stage for equivalent design speed and pressure ratio.



(a) Adiabatic efficiency.

Figure 8. - Spanwise variation of adiabatic efficiency and pressure-loss coefficient in second stage for equivalent design speed and pressure ratio.





(b) Pressure-loss coefficient across stator.

Figure 8. - Concluded. Spanwise variation of adiabatic efficiency and pressure-loss coefficient in second stage for equivalent design speed and pressure ratio.

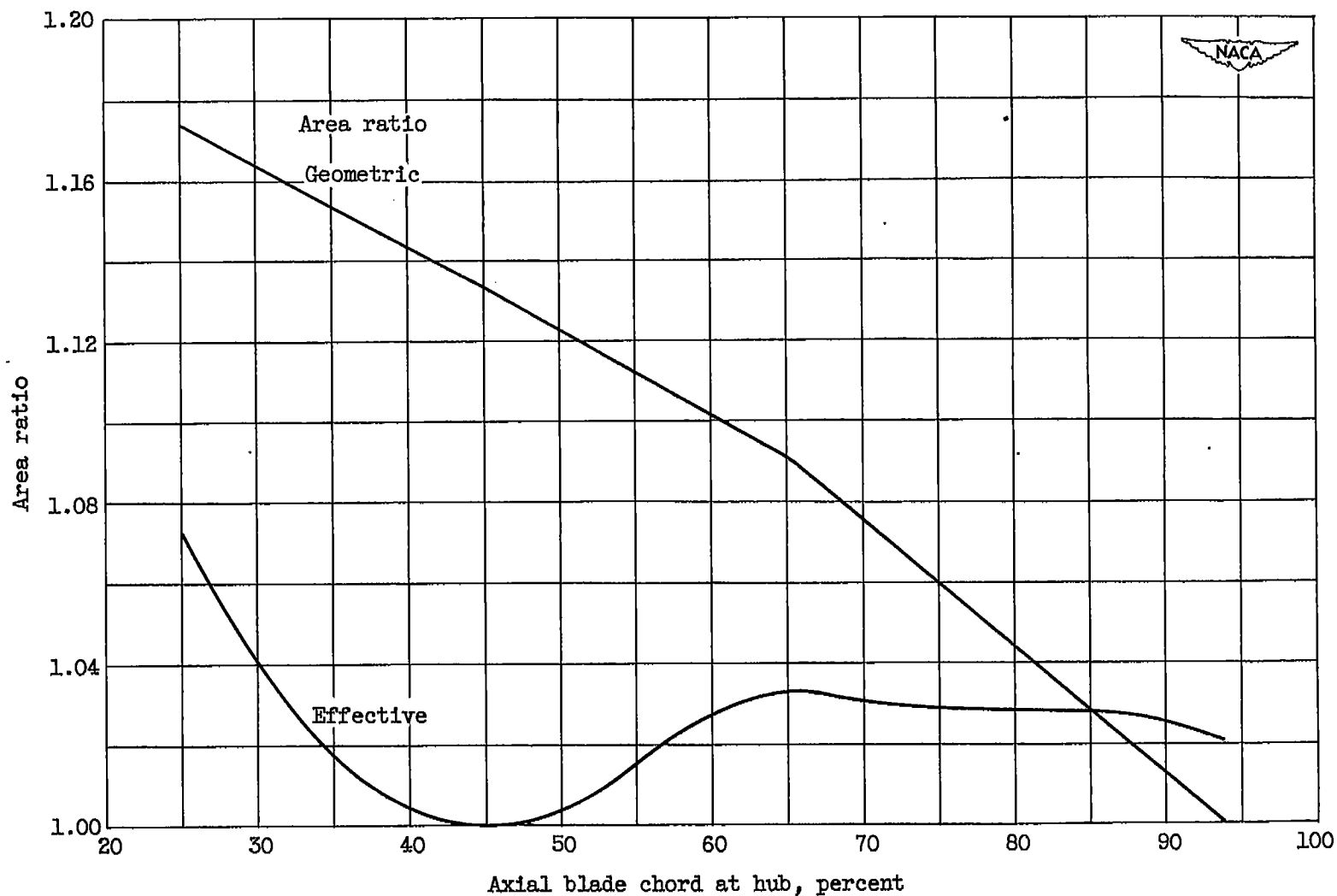


Figure 9. - Variation of geometric and effective area ratios through second-stage rotor blade passage with percentage of axial blade chord at hub.

# SECURITY INFORMATION

**[REDACTED]**



**[REDACTED]**

11

**[REDACTED]**